Trends in graphene edge properties and flake shapes: a first-principles study

Chee Kwan Gan and David J. Srolovitz
Materials Theory and Simulation Laboratory, Institute of High Performance Computing, 1 Fusionopolis Way, #16-16 Connexis, Singapore 138632, Singapore

(Dated: 24 Sep, 2009)

We use density functional theory to determine the equilibrium shape of graphene flakes, through the calculation of the edge orientation dependence of the edge energy and edge stress of graphene nanoribbons. The edge energy is a nearly linear function of edge orientation angle; increasing from the armchair orientation to the zigzag orientation. Reconstruction of the zigzag edge lowers its energy to less than that of the armchair edge. The edge stress for all edge orientations is compressive, however, reconstruction of the zigzag edge reduces this edge stress to near zero. Hydrogen adsorption is favorable for all edge orientations; dramatically lowering all edge energies and all edge stresses. It also removes the reconstruction of the zigzag edge. Using the new edge energy data, we determine the equilibrium shape of a graphene sheet (with unreconstructed edges) to be hexagonal with straight armchair edges in the presence and absence of hydrogen. However, zigzag edge reconstruction produces graphene flakes with a six-fold symmetry, but with rounded edges. This shape is dominated by near zigzag edges. The compressive edge stresses will lead to edge buckling (out-of-the-plane of the graphene sheet) for all edge orientations, in the absence of hydrogen. Exposing the graphene flake to hydrogen dramatically decreases the buckling amplitude.

PACS numbers: 61.48.-c,62.23.Kn,71.15.Mb,62.25.-g
Keywords: Graphene sheets, graphene nanoribbons, edge energy, edge stress

I. INTRODUCTION

Graphene, a one-atom thick single sheet of sp^2-bonded carbon atoms in a honeycomb lattice, is a zero-gap semiconductor (semi-metal) that exhibits extraordinarily high electron mobility and shows considerable promise for applications in electronic and optical devices, high sensitivity gas detection, ultracapacitors and biodevices[1,2,3,4,5,6,7,8,9,10,11]. Graphene can be separated from bulk graphene using a peeling technique known as mechanical exfoliation[1]. Lithography techniques[12] have recently been applied to fabricate patterned graphene nanoribbons (GNR) with widths below 100 Å; such GNR were used to produce graphene field effect transistors with on-off ratios as high as $\sim 10^7$. There has been concerted efforts to investigate the stability of graphene sheets[13,14,15,16,17,18]. Since applications of graphene necessarily employ sheets of finite extent, it is also of interest to inquire as to the equilibrium shape of such finite sheets or flakes.

Two distinct definitions of shape arise in the context of graphene sheets. The first is associated with a finite, perfectly flat graphene sheet. For such a sheet, the equilibrium shape is determined primarily by the energy of the graphene sheet edges. Edge energies are related to the thermodynamically stable shape in exactly the same way that surface energies are used to predict the equilibrium shape of a three dimensional crystal through the Wulff construction[19]. The second is associated with equilibrium elastic distortions of the graphene sheet as a result of edge stresses (analogous to surface stresses for a three-dimensional crystal). Several recent studies[15,16] have shown that the two highest symmetry graphene edges have compressive edge stresses, leading to elastic distortions of the regions near these sheet edges (edge warping). In this paper, we employ density-functional theory (DFT) to determine graphene edge energies and edge stresses as a function of edge orientation both in the absence and in the presence of hydrogen atoms. We employ these results to investigate the equilibrium shape of a finite graphene sheet; both for the flat sheet (a two-dimensional intrinsic manifold) and one for which elastic distortions are permitted (a two-dimensional sheet embedded in three dimensions).

II. CALCULATION METHODS

In order to determine the properties of the edges of graphene sheets, we employ density-functional theory (DFT)[20,21] within the local density approximation (LDA) using a self-consistent pseudopotential method, as implemented in the Siesta code[22]. A double-ζ plus polarization basis set is used for the localized basis orbitals along with a large energy cutoff (400 Ry) for the real space integration. An electronic temperature of 0.01 eV is used to smear the Fermi-Dirac distribution. In order to study graphene sheet edges, we focus on flat graphene nanoribbons (GNR) that are periodic in one direction and are separated by 16 Å of vacuum in the other two directions. In the direction parallel to the ribbon axis, we use a k-point sampling criterion such that the number of k points n_k in the periodic direction is determined by the smallest integer that fulfills $n_k L = 136.96$ Å, where L is the length of the ribbon in the periodic direction. This corresponds to a 32-k-point scheme for 4.28 Å, the dimension of the smallest unit cell of an armchair edge. We minimize the energy with respect to ionic position in the GNR plane; the relaxation is stopped when the force on each atom is less than 0.01 eV/Å. We first de-

termine the honeycomb lattice constant a_0 of the infinite graphene sheet, which is $a_0 = 2.471$ Å. This corresponds to a C-C bond length of $a_0/\sqrt{3} = 1.427$ Å. This agrees very well with the value of $a_0 = 2.468$ Å found in another density-functional calculation[23].

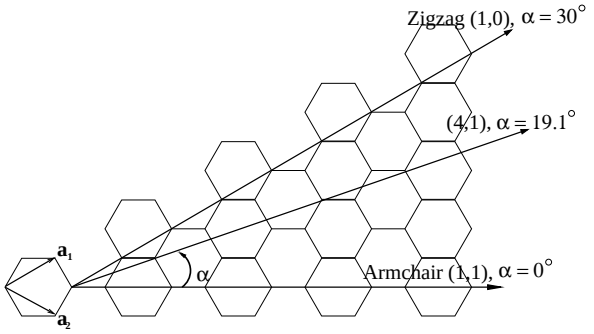

FIG. 1: A graphene edge orientation is defined by the angle α between edge tangent vector $\mathbf{T}_e = n\mathbf{a}_1 + m\mathbf{a}_2$ and the armchair vector $\mathbf{a}_{ac} = \mathbf{a}_1 + \mathbf{a}_2$. The two highest symmetry edges are shown: the $\alpha = 0°$ (1,1) armchair edge and the $\alpha = 30°$ (1,0) zigzag edge. Also show is the more general $(4, 1)$ graphene edge, corresponding to $\alpha = \cos^{-1}\left(\frac{5}{2\sqrt{7}}\right) = 19.1°$.

A general graphene edge orientation can be described by a convention that is commonly used to describe the chirality of a single-wall carbon nanotube[24]. We use α to describe the angle between the tangent to the edge $\mathbf{T}_e = n\mathbf{a}_1 + m\mathbf{a}_2$ and a second vector parallel to the armchair, as shown in Fig. 1. This angle is given by $\alpha = \cos^{-1}\sqrt{\frac{3(n+m)^2}{4[(n+m)^2-mn]}}$. Naturally, the armchair and zigzag edges correspond to $\alpha = 0°$ and $30°$, respectively. Because of the symmetry of the honeycomb lattice, we only need to consider angles within the range of $0° \leq \alpha \leq 30°$. In the present study, we study a discrete set of edge orientations in this α-range: $0°(1,1)$, $6.59°(3,2)$, $10.89°(2,1)$, $16.10°(3,1)$, $19.11°(4,1)$, $21.05°(5,1)$, and $30°(1,0)$. Figure 2b shows a $(5,1)$ graphene nanoribbon, corresponding to $\alpha = 21.05°$; each repeat period of this edge structure contains 5 zigzag units (Fig. 2c) and a kink that has the armchair structure (Fig. 2a).

In the absence of hydrogen, the edge energy (per unit length) $E_{\rm edge}$ is

$$E_{\rm edge} = \frac{1}{2L}[E_{\rm GNR}(\alpha, w) - n_{\rm C}E_1], \qquad (1)$$

where $E_{\rm GNR}(\alpha, w)$ is the energy of an optimized GNR with edge orientation α and width w that contains $n_{\rm C}$ carbon atoms, and E_1 is the energy per carbon atom in the infinite, flat graphene sheet with the lattice parameter that minimizes the energy. The factor of two in Eq. 1 accounts for the fact that a GNR has two edges. In this work, we also consider the termination of all of the dangling bonds on the unreconstructed edges by hydrogen atoms. In this case, the edge energy is

$$E_{\rm edge+H} = \frac{1}{2L}\left[E_{\rm GNR+H}(\alpha, w) - n_{\rm C}E_1 - \frac{n_{\rm H}E_{\rm H_2}}{2}\right] \qquad (2)$$

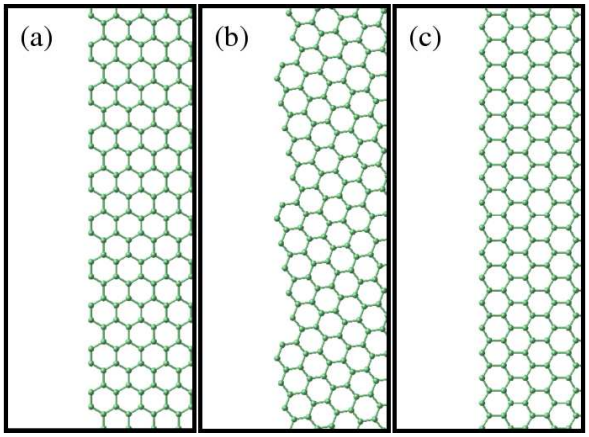

FIG. 2: (Color online) The edge structure of unreconstructed graphene sheets in the (a) armchair $\alpha = 0°$ (1,1), (b) $\alpha = 21.05°$ (5,1), and (c) zigzag $\alpha = 30°$ (1,0) orientations.

where $E_{\rm GNR+H}(\alpha, w)$ is the energy of the graphene nanoribbon where the dangling bonds associated with carbon atoms on the edge are saturated with single H atoms and $n_{\rm H}$ is the total number of such H atoms. $E_{\rm H_2}$ is the energy of the hydrogen molecule and the factor of 2 in the last term accounts for the fact that each H_2 molecule only contributes one H atom to each initially unsaturated bond. Note that Eq. 2 reduces to Eq. 1 in the absence of hydrogen $n_{\rm H} = 0$.

By analogy with the surface stress[25], we define the edge stress $\tau_{\rm e}$ as the work required to stretch a graphene edge by an infinitesimal strain ϵ (parallel to the edge), $\Delta E_{\rm edge}/\epsilon$, or in differential form by

$$\tau_{\rm e} = \frac{dE_{\rm edge}}{d\epsilon}. \qquad (3)$$

(Note: two definitions of surface stress τ_s have been widely employed in the literature: (a) $\tau_s = d\gamma/d\epsilon$ and (b) $\tau_s = \gamma + d\gamma/d\epsilon$, where γ is the surface energy. We apply the approach used for surface stress definition (a) here, i.e., $\tau_e = dE_{\rm edge}/d\epsilon$. This is consistent with the method employed by Jun[16], but not by Huang *et al.*[17] in their studies of graphene edges. This definition yields the edge stress that produces elastic distortions of graphene nanoribbon edges[15,16].) The derivative in Eq. 3 is determined using a method based upon the bulk stress calculation within the Siesta code[22] that assumes an affine transformation of the atomic coordinates according to the applied strain. Throughout this work, we adopt the convention that a negative (positive) edge stress corresponds to compression (tension).

III. EDGE ENERGY

The first question we address, is how wide must a GNR be in order that the interactions between the opposite, parallel edges are negligible. Figure 3 shows

the edge energy versus GNR width, without and with H-termination. These figures clearly demonstrate that the edge energy converges to a nearly width-independent value for $w \geq 30$ Å for all GNR orientations, both without and with H-termination. We note that earlier first principles have both included[4,17] and excluded[16,26] spin polarization effects. We have not included spin polarization effects here as they are expected to be more important for a proper determination of the band structure of zigzag edge graphene nanoribbons than for the overall edge thermodynamics.

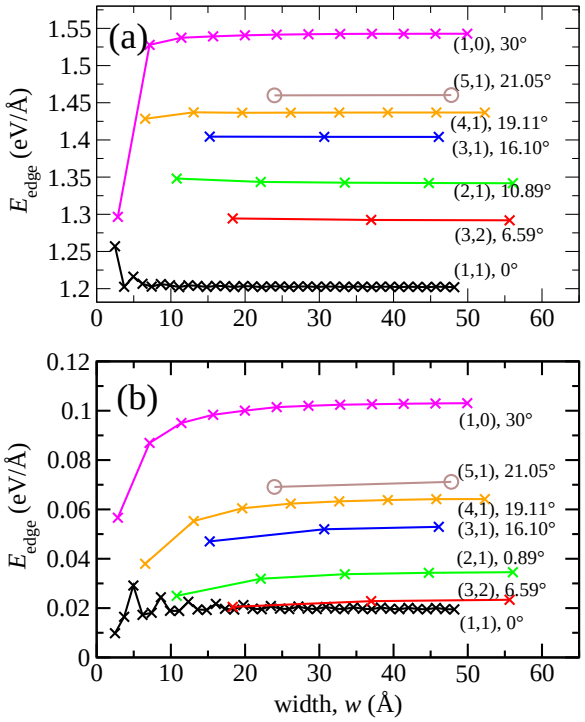

FIG. 3: (Color online) The edge energy as a function of GNR width of the unreconstructed graphene nanoribbon (a) without hydrogen termination, and (b) with hydrogen termination for several GNR edge orientations.

Unlike for all of the other edges, the $\alpha = 0°$ (1,1) armchair edge energy exhibits a decaying oscillatory behavior with respect to GNR width w, as seen in Fig. 3. This is consistent with earlier observations for the special case of an armchair GNR without H-termination[27,28]. Son *et al.*[4] demonstrated that the energy bandgap of armchair GNRs can be grouped into 3 families according to the GNR width, w. These families correspond to $N_a = 3p$, $3p+1$ and $3p+2$, where p is an integer and N_a is the number of carbon rows parallel to the armchair GNR axis. Figures 4 a and b show the edge energy versus GNR width for the unterminated and H-terminated cases, where the data has been separated according to these families. With this division, the armchair edge energy versus w largely converges monotonically.

The converged (with respect to w) edge energies shown in Fig. 3 are summarized in Fig. 5a as a function of

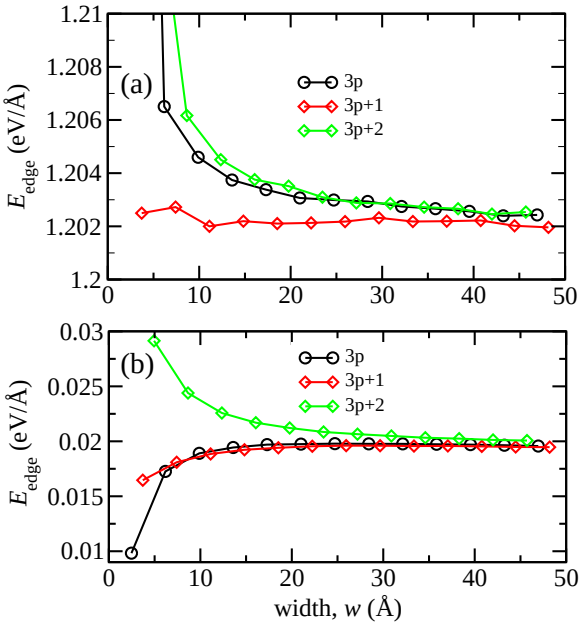

FIG. 4: (Color online) The $\alpha = 0°$ (1,1) armchair edge as a function of ribbon width w grouped according to the division of the data into three families[4] (a) without hydrogen termination and (b) with hydrogen termination.

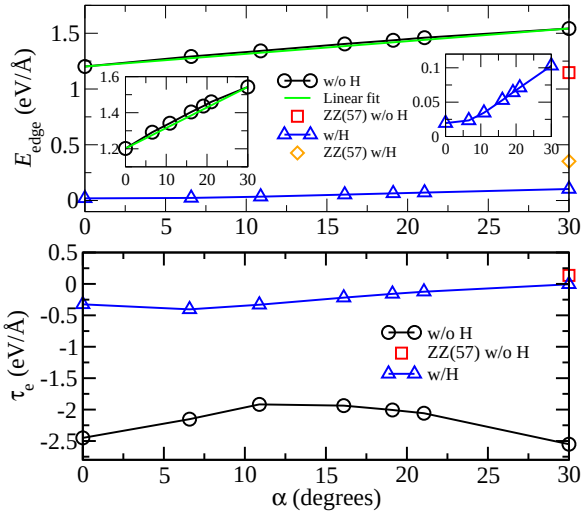

FIG. 5: (Color online) (a) The graphene edge energy as a function of the edge orientation α for the largest width GNRs in Fig. 3. The insets show the same data as in the main figure but over a narrower edge energy range. The figure shows data for the unreconstructed edges both without and with H-termination. Also shown are data points for the reconstruction of the $\alpha = 30°$ (1,0) zigzag edges [ZZ(57)] without and with H-termination. (b) The edge stress as a function of edge orientation α for the same configurations as in (a). The hydrogenated zigzag(57) has too large of a tensile edge stress, 2.570 eV/Å to show on this plot.

edge type, α. For the unreconstructed and unterminated edges, this data shows that the edge energy increases nearly linearly with α; the armchair (zigzag) edge has the lowest (highest) edge energy, 1.202 eV/Å (1.543 eV/Å). The energy ordering (armchair versus zigzag) can be understood by noting that the armchair edge reduces its energy by forming triple bonds in the armrest regions, as suggested by the fact that this bond length 1.258 Å is much smaller that the bulk graphene C-C bond length of 1.427 Å. In contrast, the zigzag edge does not have the opportunity to form triple bonds; the outer C-C bonds relax slightly to yield a bond length of 1.400 Å. The edge energy difference between the armchair and zigzag edges is 0.341 eV/Å without reconstruction or H-termination, in agreement with previous DFT results[26] (0.33 eV/Å). The near linearity of the edge energy with respect to α can be understood by noting that all of the unreconstructed edges are made up of a combination of armchair and zigzag units in proportion to the edge angle; i.e., steps on near armchair oriented edges are zigzag units and steps on near zigzag oriented edges are armchair units (see the (5,1) edge in Fig. 2).

IV. EDGE STRESS

The graphene edge stresses, with and without hydrogen termination, are presented in Fig. 5b. Without hydrogen termination, the edge stresses are compressive (negative) for all α. For the armchair [$\alpha = 0°$, (1,1)] edge $\tau_e = -2.451$ eV/Å and for the zigzag [$\alpha = 30°$, (1,0)] edge $\tau_e = -2.551$ eV/Å. These values are of the same order of magnitude as those obtained by Jun[16] (i.e., armchair edge - $\tau_e = -2.640$ eV/Å and zigzag edge - $\tau_e = -2.248$ eV/Å). Calculations of the edge stresses using an adaptive intermolecular reactive empirical bond order (AIREBO) potential, significantly underestimate the magnitude of the armchair and zigzag edge stresses (i.e., they find that the edge stresses of the armchair and zigzag edges are $\tau_e = -1.05$ eV/Å and $\tau_e = -2.05$ eV/Å, respectively). While earlier studies only considered the edge stresses of the two highest symmetry edges, the results of Fig. 5b show the edge energy for many intervening orientations. Unlike for the edge energies, the edge stress is not a monotonic function of the edge orientation angle. Rather, the magnitude of the edge stress is a minimum at $\alpha \sim 15°$. Reconstruction of the zigzag edge to from the zigzag(57) structure considerably raises the zigzag edge stress to near zero (slightly tensile).

The main conclusion from this part of the study is that in the absence of hydrogen, all edge orientations exhibit compressive edge stresses (except for the zigzag edge upon reconstruction). We can understand the sign of the edge stress by consideration of edge relaxation (i.e., like surface relaxation). Finnis and Heine[29] presented an argument in which surface atoms relax inward (toward the bulk) in order to smooth the electron density near the surface. This lowers the kinetic energy of the electrons, while having a relatively weak effect on the pseudopotential contribution to the total energy. The same thing happens at edges in the present two dimensional material. When the edge atoms move inward, they create a force on the atoms below the edge that is parallel to the edge and tends to push these atoms apart. However, the atom spacing, parallel to the edge, is fixed by the constraint of the atoms in the bulk of the graphene sheet. It is these forces that create the compressive edge stress. When hydrogen adsorbs on the surface (see below), the inward relaxation effect is strongly reduced (due to near perfect saturation of the dangling bonds), thereby greatly reducing the magnitude of the compressive edge stresses.

V. HYDROGEN ADSORPTION

When hydrogen terminates all of the dangling bonds of the ribbon edges, the unreconstructed edge energies drop by $1-2$ orders of magnitude, as seen in Figs. 3b and 5a. The edge energy in the presence of hydrogen is maximum for the zigzag [$\alpha = 30°$, (1,0)] edge ($E_{edge} = 0.103$ eV/Å) and minimum for the armchair [$\alpha = 0$, (1,1)] edge ($E_{edge} = 0.019$ eV/Å). While the magnitude of the edge energies drop dramatically upon hydrogen saturation, the ratio of the zigzag to armchair energies shows a much smaller change.

Saturating the GNR edges with hydrogen significantly decreases the magnitude of the edge stresses (see Fig. 5b). Interestingly, saturating the zigzag GNR edge with hydrogen changes the edge stress from highly compressive, -2.551 eV/Å, to nearly zero, -0.006 eV/Å. This is consistent with the results of an earlier study[16] that show a significant drop in the magnitude of the edge stress upon saturating the edges with hydrogen.

In order to understand the effect of hydrogen on the GNR edges, we focus first on the hydrogen adsorption energy E_{ads} on the graphene edge: $E_{ads} = (E_{GNR} + n_H E_H - E_{GNR+H})/n_H$. If we denote the number of H atoms adsorbed per unit length of the edge as $\eta_H = n_H/2L$, and the binding energy of the hydrogen molecule (relative to the isolated hydrogen atoms) as $E_b = 2E_H - E_{H_2}$, we can rewrite E_{edge+H} (see Eq. 2) as

$$E_{edge+H} = E_{edge} - \eta_H(E_{ads} - \frac{E_b}{2}). \quad (4)$$

This change in edge energy (per unit length) upon saturation with hydrogen is simply the product of the number of H atoms adsorbed (per unit length) and the change in energy per hydrogen atom in going from H_2 in the gas to H on the edge. For the unreconstructed edges of graphene, η_H has a very simple form:

$$\eta_H = \frac{\cos\alpha}{a_0}\sqrt{\frac{4}{3}}, \quad (5)$$

where a_0 is the honeycomb lattice constant. η_H is 15.5%

larger for the armchair ($\alpha = 0°$) than for the zigzag edge ($\alpha = 30°$).

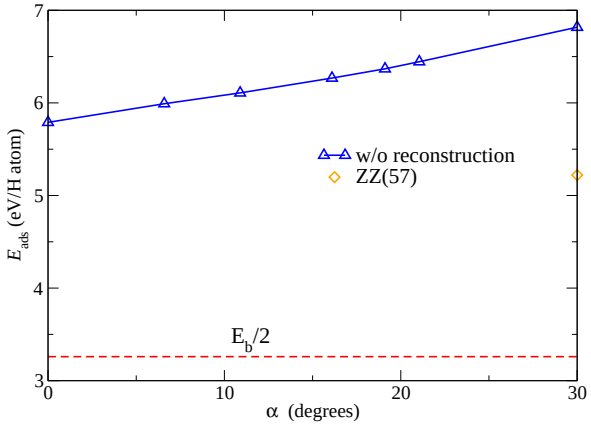

FIG. 6: (Color online) The hydrogen adsorption energy as a function of angle α. The binding energy of a hydrogen atom in H_2, $E_b/2$, is shown for reference.

The main effect of adsorbing hydrogen on the edges is to decrease the edge energy by $\eta(E_{\rm ads} - E_{\rm b}/2)$. Figure 5a shows that the energy of the zigzag edge decreases upon hydrogen adsorption more so than does the energy of the armchair edge. This is contrary to what we should expect based upon the number of adsorbed hydrogen atoms per unit length, $\eta_{\rm H}$ (which decreases with increasing α as $\cos\alpha$). However, the hydrogen adsorption energy $E_{\rm ads}$ increases with increasing α (as seen in Fig. 6) more quickly than $\eta_{\rm H}$ decreases. This effect is associated with the fact that, before hydrogen termination, carbon atoms on the armchair edge have triple bonds to neighboring edge carbon atoms (and no dangling bonds), while the zigzag edge has no triple bonds (but does have dangling bonds)[26]. This suggests that hydrogen should bind more strongly to the zigzag edge atoms than to the armchair edge atoms. This implies $(E_{\rm GNR} - E_{\rm GNR+H})/n_{\rm H}$ will be larger for the zigzag edge than for the armchair edge. Because the only term in $E_{\rm ads}$ that depends on edge type is $(E_{\rm GNR} - E_{\rm GNR+H})/n_{\rm H}$, this implies higher H adsorption energy to the zigzag edge than to the armchair edge.

The hydrogen adsorption energy on the zigzag(57) edge, 5.22 eV/atom, is significantly smaller than the adsorption energy on the unreconstructed zigzag edge (see Fig. 6). This can be attributed to the fact that triple bonds formed in the heptagonal units on the zigzag(57) edge and to the lack of triple bonds on the unreconstructed zigzag edge. The difference in adsorption energy between the two zigzag edges explains why the hydrogenated zigzag(57) edge energy is (0.249 eV/Å) higher than the hydrogenated unreconstructed zigzag edge (see Fig. 5a). It is important to focus upon H adsorption energy $E_{\rm ads}$ for the zigzag and hydrogenated zigzag edges (presented above) *relative* to the binding energy of hydrogen in molecular hydrogen $E_{\rm b}/2$ (on a *per atom* basis). This comparison shows that while reconstruction reduces the tendency for H-passivation of the zigzag edge, H will still bind to this edge. (This conclusion differs from the interpretation of the discussion in Ref. 26.)

VI. EQUILIBRIUM GRAPHENE SHEET SHAPE

In this section, we investigate the equilibrium shape of a flat graphene sheet, following a procedure akin to that used for determining the equilibrium shape of a 3-dimensional crystal via the Wulff construction (e.g., see Ref. 19). The first step is to construct a polar plot of the edge energy $E_{\rm edge}$ as a function of the edge orientation angle α. This is shown in Fig. 7a for the case of pure, unreconstructed graphene edges using the data from Fig. 5a. Next, we construct a ray from the origin at edge orientation angle α on this polar plot. Then, we draw a line perpendicular to this ray at the point of its intersection with $E_{\rm edge}$. This process is repeated for every point (many points) around the polar $E_{\rm edge}$ versus α plot. The inner envelope of these lines represents the equilibrium graphene flake shape. This construction and the resultant equilibrium flat graphene flake shape (i.e., that which minimizes the edge energy at fixed flake area) is shown in Fig. 7a for the case of graphene with no edge reconstruction and without hydrogen termination. The equilibrium shape is a hexagon with flat (1,1) armchair edges.

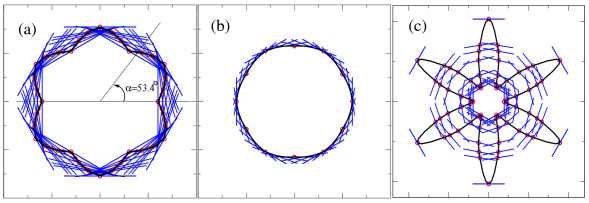

FIG. 7: (Color online) Polar plots of the graphene edge energy $E_{\rm edge}$ as a function of α (a) for edges without hydrogen termination or reconstruction, (b) with reconstruction but without hydrogen termination based upon a linear interpolation of the equilibrium armchair and zigzag(57) edge energies and (c) with hydrogen termination (no reconstruction occurs). The edge energy scales in (a) and (b) are identical, but are multiplied by a factor of 16.7 in (c) for clarity. The red circles indicate data from our density functional calculations, the black lines are an interpolation of the data and the blue lines are drawn as perpendiculars to the radius $E_{\rm edge}$ vectors. The equilibrium, flat graphene flake shape is the inner envelope of the blue lines.

The data presented in Fig. 5a suggests that, in the absence of hydrogen, the zigzag edge reconstructs and that the reconstructed surface has lower energy than even the armchair edge (which does not reconstruct). Since we do not have data for the reconstruction of all edges with $0° < \alpha < 30°$, we make the simplifying assumption that the energies of these edges can be represented by a linear interpolation between the energies of the unreconstructed $\alpha = 0°$ armchair edge and that of the reconstructed $\alpha = 30°$ zigzag(57) edge (as holds for the un-

reconstructed edges - see Fig. 5a). The resultant polar $E_{\rm edge}$ versus α plot is shown in Fig. 7b. Unlike the polar $E_{\rm edge}$ versus α plot for the unreconstructed case, this one is relatively smooth and nearly circular, yet a six-fold symmetry is obvious. Performing the Wulff construction on this interpolated $E_{\rm edge}$ versus α plot produces an equilibrium graphene flake shape that has six-fold symmetry, but no flat surfaces. The absence of flat surfaces or facets can be traced to the fact that the polar $E_{\rm edge}$ versus α plot here shows no sharp cusps (discontinuity of slope). More interesting, however, is that when we allow edge reconstruction to occur (in the absence of hydrogen), the resultant six-fold equilibrium shape is rotated relative to that without edge reconstruction. That is, the equilibrium graphene flake shape is dominated by surfaces at or near the zigzag edge orientation.

When hydrogen is introduced into the system, such that all of the dangling bonds on the edges are saturated, the edge energy is greatly reduced, as discussed above. The hydrogenation of the edges removes any reconstruction and the (1,1) armchair 0° (1,1) edge has the lowest edge energy and the zigzag 30° (1,0) edge has the highest. The resultant polar plot of $E_{\rm edge}$ versus α is shown in Fig. 7c. This plot shows strong cusps at the armchair orientations. Performing the Wulff construction, we find that the equilibrium graphene flake shape is hexagonal with (1,1) armchair edges, as in the unreconstructed, unhydrogenated graphene edge case.

The above analysis focused on the equilibrium shape of a flat, finite graphene sheet (a two-dimensional intrinsic manifold). However, a flat graphene flake is unstable against thermal rippling at finite temperature[30]. Compressive edge stresses can also lead to elastic distortions of/near the graphene flake/ribbon edges, as discussed in the literature[13,15,31]. These distortions may be described as the buckling of the edges, associated with the compressive edge stress but constrained by the elasticity of the interior of the graphene flake. The amplitude of the buckling A has been described[15] as

$$A = \left(\frac{-\lambda \tau_{\rm e}}{(\pi \sqrt{20 + 14\sqrt{7}}/18) M} \right)^{1/2} \qquad (6)$$

where λ is the wavelength of the buckling, $M = Y_b/(1-\nu^2)$, Y_b and ν are the Young's modulus and the Poisson ratio of the graphene sheet, and where we have neglected the relatively minor effect of the elastic stiffness of the edge. Assuming a typical wavelength of $\lambda = 10$ nm and $M = 2000$ eV/nm^2 for graphene[15], we can use the data presented above to determine the buckling amplitude A as a function of edge orientation α and examine the effect of hydrogenation of the edge.

Figure 8 shows the buckling amplitude from Eq. (6) using the edge stress data from Fig. 5b as a function of α, with and without hydrogen on the edges. The edge buckling amplitude found here is 3.05 and 3.11 Å for the unreconstructed armchair and zigzag edges without hydrogen, respectively, which is roughly consistent with the magnitude of the buckling amplitude reported in Ref. 15. The buckling amplitude is in the range of 2.70 to 3.11 Å over the entire range of α for the unreconstructed edges without hydrogen. Interestingly, if the zigzag edge reconstructs to the (57) structure, the buckling amplitude, as per Eq. (6), is imaginary (the edge stress is positive); implying that the reconstructed zigzag edge does not buckle.

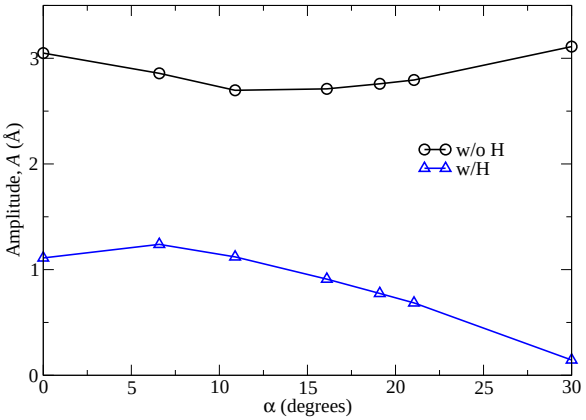

FIG. 8: (Color online) The edge buckling amplitude for the pure and hydrogenated, unreconstructed edges, as per Eq. 6 using the data from Fig. 5b.

When the edges are saturated with hydrogen, the edge stress drops dramatically (by a factor of ~ 7.54 to 425 for the armchair and zigzag edges, respectively) and the buckling amplitude drops to 1.11 and 0.14 Å for the armchair and zigzag edges (see Fig. 8). This represents a drop in edge buckling amplitude by a factor of ~ 2.3 to 22. In short, edge hydrogenation strongly reduces the edge stress driven graphene edge buckling to the point that it is, for most purposes, negligible.

VII. CONCLUSIONS

We have employed density functional theory-based calculations of graphene nanoribbons to determine the edge orientation dependence of the edge energy and edge stress (akin to surface stress in three-dimensional materials). In the absence of reconstruction, the edge energy is a nearly linear function of edge orientation angle; increasing from the armchair orientation to the zigzag orientation. Reconstruction of the zigzag edge, however, lowers its energy to less than that of the armchair edge. The edge stress for all edge orientations is compressive. The magnitude of the edge stress is a minimum at an orientation nearly midway between the armchair and zigzag orientations. Reconstruction of the zigzag edge reduces the edge stress to near zero (very slightly tensile). Hydrogen adsorption to graphene edges is favorable for all edge orientations, with a larger adsorption energy to the unreconstructed zigzag edge than to the armchair. Hydrogen adsorption dramatically lowers all edge energies

and all edge stresses. It also removes the reconstruction of the zigzag edge.

The thermodynamic properties of graphene edges play a key role in determining the equilibrium shape of a finite graphene sheet or flake. Using the new edge energy data, we determined that the equilibrium shape of a graphene sheet (with unreconstructed edges) is hexagonal with straight armchair edges. This result is valid for both the hydrogen-free case with unreconstructed edges and in the presence of hydrogen. However, if the zigzag edges reconstruct (as thermodynamically favored), graphene flakes will have a six-fold symmetry, but with rounded (rather than faceted) edges. Interestingly, the six-fold symmetry is rotated with respect to the hydrogenated case and will be dominated by near zigzag edges.

The compressive edge stresses will lead to edge buckling (out-of-the-plane of the graphene sheet) for all edge orientations, in the absence of hydrogen. The edge buckling amplitude is expected to be approximately 3 Å, but this value depends on buckling wavelength. Exposing the graphene flake to hydrogen will dramatically decrease the buckling amplitude to the point that it may be too small to be of any significance.

VIII. ACKNOWLEDGMENT

The authors gratefully acknowledge useful discussions with Paulo Branicio, Yong Wei Zhang, and Nathaniel Ng. The basis sets and pseudopotentials were provided by Young-Woo Son and Su Ying Quek. We are also grateful to Julian Gale for his input on the use of the Siesta code.

[1] K. S. Novoselov, A. K. Geim, S. V. Morozov, D. Jiang, Y. Zhang, S. V. Dubonos, I. V. Grigorieva, and A. A. Firsov, Science **306**, 666 (2004).
[2] Y. Zhang, Y. Tan, H. L. Stormer, and P. Kim, Nature **438**, 201 (2005).
[3] K. S. Novoselov, A. K. Geim, S. V. Morozov, D. Jiang, M. I. Katsnelson, I. V. Grigorieva, S. V. Dubonos, and A. A. Firsov, Nature **438**, 197 (2005).
[4] Y. W. Son, M. L. Cohen, and S. G. Louie, Phys. Rev. Lett. **97**, 216803 (2006).
[5] F. Schedin, A. K. Geim, S. V. Morozov, E. W. Hill, P. Blake, M. I. Katsnelson, and K. S. Novoselov, Nat Mater **6**, 652 (2007).
[6] A. K. Geim and K. S. Novoselov, Nature Materials **6**, 183 (2007).
[7] N. Mohanty and V. Berry, Nano Letters **8**, 4469 (2008).
[8] M. D. Stoller, S. Park, Y. Zhu, J. An, and R. S. Ruoff, Nano Letters **8**, 3498 (2008).
[9] T. Echtermeyer, M. Lemme, M. Baus, B. Szafranek, A. Geim, and H. Kurz, Electron Device Letters, IEEE **29**, 952 (2008).
[10] A. H. CastroNeto, F. Guinea, N. M. R. Peres, K. S. Novoselov, and A. K. Geim, Rev. Mod. Phys. **81**, 109 (2009).
[11] A. K. Geim, Science **324**, 1530 (2009).
[12] X. Li, X. Wang, L. Zhang, S. Lee, and H. Dai, Science **319**, 1229 (2008).
[13] J. C. Meyer, A. K. Geim, M. I. Katsnelson, K. S. Novoselov, T. J. Booth, and S. Roth, Nature **446**, 60 (2007).
[14] T. Wassmann, A. P. Seitsonen, A. M. Saitta, M. Lazzeri, and F. Mauri, Phys. Rev. Lett. **101**, 096402 (2008).
[15] V. B. Shenoy, C. D. Reddy, A. Ramasubramaniam, and Y. W. Zhang, Phys. Rev. Lett. **101**, 245501 (2008).
[16] S. Jun, Phys. Rev. B **78**, 073405 (2008).
[17] B. Huang, M. Liu, N. Su, J. Wu, W. Duan, B. lin Gu, and F. Liu, Phys. Rev. Lett. **102**, 166404 (2009).
[18] C. O. Girit, J. C. Meyer, R. Erni, M. D. Rossell, C. Kisielowski, L. Yang, C.-H. Park, M. F. Crommie, M. L. Cohen, S. G. Louie, et al., Science **323**, 1705 (2009).
[19] A. Pimpinelli and J. Villain, *Physics of Crystal Growth* (Cambridge University Press, United Kingdom, 1998).
[20] P. Hohenberg and W. Kohn, Phys. Rev. **136**, 864B (1964).
[21] W. Kohn and L. J. Sham, Phys. Rev. **140**, 1133A (1965).
[22] J. Soler, E. Artacho, J. D. Gale, A. García, J. Junquera, P. Ordejón, and D. Sánchez-Portal, J. Phys.: Condens. Matter **14**, 2745 (2002).
[23] S. Reich, J. Maultzsch, C. Thomsen, and P. Ordejón, Phys. Rev. B **66**, 035412 (2002).
[24] R. Saito, G. Dresselhaus, and M. S. Dresselhaus, *Physical Properties of Carbon Nanotubes* (Imperial College Press, London, 1998).
[25] J. W. Gibbs, *The Scientific Papers of J. Willard Gibbs*, vol. 1 (Longmans-Green, London, 1906).
[26] P. Koskinen, S. Malola, and H. Hakkinen, Phys. Rev. Lett. **101**, 115502 (2008).
[27] T. Kawai, Y. Miyamoto, O. Sugino, and Y. Koga, Phys. Rev. B **62**, R16349 (2000).
[28] M. Fujita, M. Igami, and K. Nakada, J. Phys. Soc. Japan **66**, 1864 (1997).
[29] M. W. Finnis and V. Heine, J. Phys. F **4**, L37 (1973).
[30] A. S. Barnard and I. K. Snook, J. Comp. Phys. **128**, 094707 (2008).
[31] A. Fasolino, J. H. Los, and M. I. Katsnelson, Nat Mater **6**, 858 (2007).